ACS OMEGA

Article

Cite This: ACS Omega 2019, 4, 3946−3953

http://pubs.acs.org/journal/acsodf

Preparation and Dye Degradation Performances of Self-Assembled MXene-Co_3O_4 Nanocomposites Synthesized via Solvothermal Approach

Shanshan Luo,[†,‡] Ran Wang,[‡] Juanjuan Yin,[‡] Tifeng Jiao,*[,†,‡] Kaiyue Chen,[‡] Guodong Zou,[†] Lun Zhang,[‡] Jingxin Zhou,[‡] Lexin Zhang,[‡] and Qiuming Peng[†]

[†]State Key Laboratory of Metastable Materials Science and Technology and [‡]Hebei Key Laboratory of Applied Chemistry, School of Environmental and Chemical Engineering, Yanshan University, 438 West Hebei Street, Qinhuangdao 066004, China

ABSTRACT: Two-dimensional metal carbides or nitrides (MXenes) demonstrated wide applications in energy storage, water treatment, electromagnetic shielding, gas/biosensing, and photoelectrochemical catalysis due to their higher specific surface area and excellent conductivity. They also have the advantages of flexible and adjustable components and controllable minimum nanolayer thickness. In this study, a cube-like Co_3O_4 particle-modified self-assembled MXene (Ti_3C_2) nanocomposite has been prepared successfully by a simple solvothermal method. The Co_3O_4 particles are well dispersed on the surface and inner layers of the Ti_3C_2 sheets, which effectively prevent the restacking of Ti_3C_2 sheets and form an organized composite structure. The physical properties of these nanocomposites were studied by using XRD, SEM, EDX, TEM, and XPS. The performance of the obtained samples was evaluated as new nanocatalysts for degrading methylene blue and Rhodamine B in batch model experiments. The prepared Mxene-Co_3O_4 nanocomposites can be well regenerated and reused for eight consecutive cycles, indicating potential wide applications in wastewater treatment and composite materials.

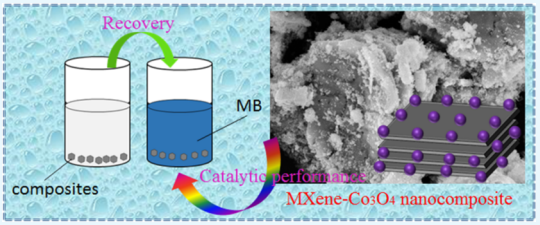

1. INTRODUCTION

Two-dimensional materials have unique electrical, optical, and mechanical properties. MXene is a new type of two-dimensional crystalline compound with graphene-like structure and novel properties.[1] It is one of the stars in the field of functional materials research in recent years. It is peeled off by MAX phase etching.[2] The MAX phase is a ternary-layered carbide or nitride material that combines the properties of both metals and ceramics.[3] The MAX phase has the general formula $M_{n+1}AX_n$, where M is a transition metal element, A is mainly a group IIIA or IVA element, X is carbon and/or nitrogen, and n = 1, 2, or 3. So far, more than 70 MAX phases have been discovered.[4] The MAX phase is a hexagonal crystal structure, the M atomic layer is closely packed, the X atom is filled in the M atom octahedron, and the M atomic layer is interspersed in the A atomic layer. It could be thought that the MAX phase is bonded by a two-dimensional layered carbide/nitride to the A atomic layer. Among them, M−A is a mixture of covalent bond/metal bond/ion bond, and M−X is a covalent bond.[5] Thus, the A atomic layer is removed by etching, and a two-dimensional MXene nanosheet is obtained by liquid phase stripping.[6,7] In addition, the thickness of a single MXene layer can reach 1 nm, and the area diameter can reach several tens of micrometers.[8] The corresponding structures of MXene are also different from MAX phases with different n values. Nineteen kinds of MXene have been successfully prepared, and dozens of MXene have predictive stability in theory; this diversified structural composition provides a broad space for its property regulation and derivative material construction.

Moreover, the Co_3O_4 crystal exhibited a normal spinel structure, namely, $Co^{2+}(Co^{3+})_2O^{2-}{}_4$, where O^{2-} is in a densely packed cubic structure, Co^{2+} is located in its tetrahedral gap, and Co^{3+} is located in its octahedral gap with higher crystal field stabilization energy. When the air is lower than 800 °C, the properties are very stable. At room temperature, it is not easily soluble in various concentrated acids and water but could be dissolved in a hot sulfuric acid solution at a lower rate. In addition, it is also a p-type semiconductor material. It also has a very wide range of applications, such as sensors,[9] supercapacitors,[10] catalysts,[11−19] magnetic semiconductors,[20] and rechargeable battery materials.[21−23] For example, Huang et al. synthesized silver nanoparticle-modified MXene composites by self-reduction reactions with enhanced catalytic performances.[11] Yang et al. used a simple pyrolysis method to prepare Co_3O_4 nanoparticles/nitrogen-doped carbon composites with different structures for oxygen evolution.[12] Chen et al. skillfully used a multistep method to synthesize mesoporous Co_3O_4 and carbon nanotube composites with a layered pipe structure as a negative electrode material for lithium ion batteries.[13] This unique nanostructure solved the problem of volume expansion and low electron conductivity of metal oxide anodes.[24] Moreover, some similar composites exhibit excellent performance in electrochemistry and wide applications.[25−31]

Received: January 25, 2019
Accepted: February 12, 2019
Published: February 21, 2019

DOI: 10.1021/acsomega.9b00231
ACS Omega 2019, 4, 3946−3953

Dyes are widely used in various industries, among which methylene blue (MB) is often used in the printing and dye industry as an important target for wastewater treatment.[32−39] It is reported to be carcinogenic and mutagenic, which may be harmful to plants and animals. Rhodamine B (RhB) is also a kind of widely used dye. Therefore, the removal of MB and RhB from wastewater causes widespread concern. Herein, we proposed to synthesize Co_3O_4 particle-modified MXene (Mxene-Co_3O_4) nanocomposites by an in situ solvothermal method. The Co_3O_4 nanocomposites were uniformly anchored on the surface of Ti_3C_2 sheets, which enhanced the catalytic activity. At the same time, the close interaction between the Co_3O_4 component and the Ti_3C_2 substrate promoted the performance improvement of the catalyst. The prepared Mxene-Co_3O_4 nanocomposites showed good performance for catalytic degradation of methylene blue and Rhodamine B as model dyes. The present work on Mxene-Co_3O_4 nanocomposites had demonstrated a new clue for the research field of MXene composite catalysis.

2. RESULTS AND DISCUSSION

2.1. Characterization of MXene-Co_3O_4 Nanocomposites. Herein, the targeted sheet-like nanomaterial MXene-Co_3O_4 was prepared by a simple solvothermal method, as shown in Figure 1. The first part is the synthesis of Mxene-

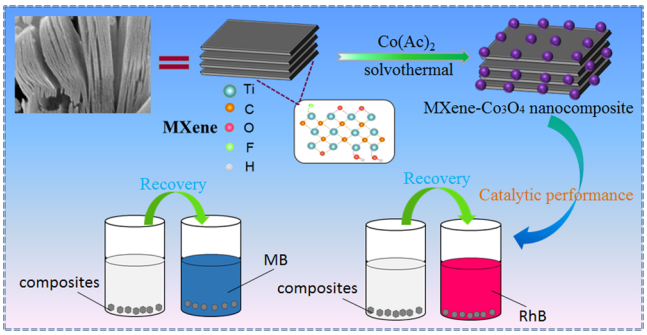

Figure 1. Schematic illustration of the synthesis and catalytic process of MXene-Co_3O_4 nanocomposites.

Co_3O_4 composites. MXene was made of Ti_3AlC_2 type MAX ceramics and etched with a mixed solution of HCl (6 M) and LiF (2.5 M) in aqueous solution under ultrasonication. The other part is the catalytic degradation of dyes, such as methylene blue (MB) and Rhodamine B (RhB), by MXene-Co_3O_4 nanocomposites. In this work, we chose two catalysts, namely, MXene-Co_3O_4 and Co_3O_4, and then selected the catalyzed dyes.

Figure 2 shows the microscopic morphology of MXene-Co_3O_4, Co_3O_4, and MXene. From Figure 2a,b, it could be seen that MXene had a well-fabricated accordion morphology. Pure Co_3O_4 showed a small cube type, which had an average crystallite size of 20 nm. Figure 2c,d shows the TEM and SEM images of the MXene-Co_3O_4 composites. It could be clearly seen that the surface of MXene was coated with a large amount of Co_3O_4 particles, and a small amount of Co_3O_4 could enter the layer of MXene, which indicated that this is beneficial to the catalytic degradation of methylene blue and Rhodamine B. It could be explained that the formed MXene-Co_3O_4 composite has a larger specific surface area, which was advantageous for the adsorption of dyes and could be used for catalytic experiments. Energy dispersive X-ray (EDX) spectroscopy (inset in Figure 2c) confirms that the elemental composition of the composite consists solely of carbon, titanium, cobalt, and oxygen, whose proportions were consistent to form MXene-Co_3O_4. In addition, Figure 3 describes the elemental mappings of the prepared MXene-Co_3O_4 composite. According to C, Ti, and Co images, the data further illustrated the good distribution of the Co element on the surface of MXene after the successful solvothermal process.

X-ray powder diffraction (XRD) analysis identifies the formation of MXene-Co_3O_4 nanocomposites, as shown in Figure 4. A set of (111), (110), (223), and (440) peaks at 17.9, 25.1, 59.8, and 64.6° appeared, respectively. The disappearance of the (006) peak from Ti_3C_2 MXene suggested the suppressed restacking of MXene sheets by the Co_3O_4 nanostructure standing on its surface (Figure 2c). The other peaks originated from MXene were quite weak even in pristine MXene, for being easily overlapped by the signals from the Co_3O_4 nanostructure. After the Co_3O_4 assembly process, three distinct characteristic peaks of Co_3O_4 particles could also be found in the formed composite, that is, (111), (511), and (440) crystal planes (JCPDS number 090418), indicating that a large number of Co_3O_4 particles were adsorbed on the surface of the MXene during the solvothermal treatment process.

The thermogravimetric curve showed that the mass changes with the change of temperature, as shown in Figure 5. While Co_3O_4 was relatively stable in the test temperature range, the weight loss was attributed to the change in Ti_3C_2. It could be concluded from the curve that the weight loss of as-prepared MXene-Co_3O_4 composites from room temperature to 200 °C was mainly due to the adsorption of water. When the temperature was gradually increased, the weight loss was mainly due to the decomposition of the oxygen-containing functional groups in which the Co_3O_4 and MXene complexes were bonded to each other and the decomposition of Ti_3C_2.

Moreover, Figure 6 shows the XPS spectra of MXene and the MXene-Co_3O_4 composite. Figure 6a shows the characteristic peaks in the curve of the MXene-Co_3O_4 nanocomposite, such as Co2p, O1s, C1s, and Ti2p. Compared with pure MXene, the peak of O1s of MXene-Co_3O_4 increased obviously. It could be seen that the results of XPS are consistent with the Co, C, Ti, and O elements in the elemental EDX analysis. In addition, for the Co2p XPS spectrum in Figure 6b, it showed a low energy band ($Co2p_{3/2}$). This low energy band could be convolved into two peaks: 779.8 and 781.3 eV.[40,41] The $Co2p_{3/2}$ peak position (Figure 6b) was in accordance with the presence of Co_3O_4.[42] The analysis results were consistent with XRD, which proved the generation of Co_3O_4.

2.2. Catalytic Performances of MXene-Co_3O_4 Nanocomposites. The catalytic performance of the obtained composites was assessed by catalytic reduction of model dyes. In the present study, the catalytic reaction was carried out in a 250 mL glass flask containing 100 mL of MB dye solution (12.5 mg/L) or 100 mL of RhB (5 mg/L) and 10 mg of catalyst in the presence of 15 mL of H_2O_2 (30%) at room temperature with continuous stirring. The supernatant was centrifuged at given time intervals, and the residual dye concentrations at different time intervals were investigated by UV−visible spectroscopy using different absorption wavelengths (MB 664 nm, RhB 554 nm). In this study, catalytic reductions of MB or RhB from Co_3O_4 particles and MXene-Co_3O_4 composites were also investigated. Meanwhile, the dye removal rate was calculated according to the following formula: $K\ (\%) = (A_0 - A_T)/A_0 \times 100$,[43] where K is defined as the dye

DOI: 10.1021/acsomega.9b00231
ACS Omega 2019, 4, 3946−3953

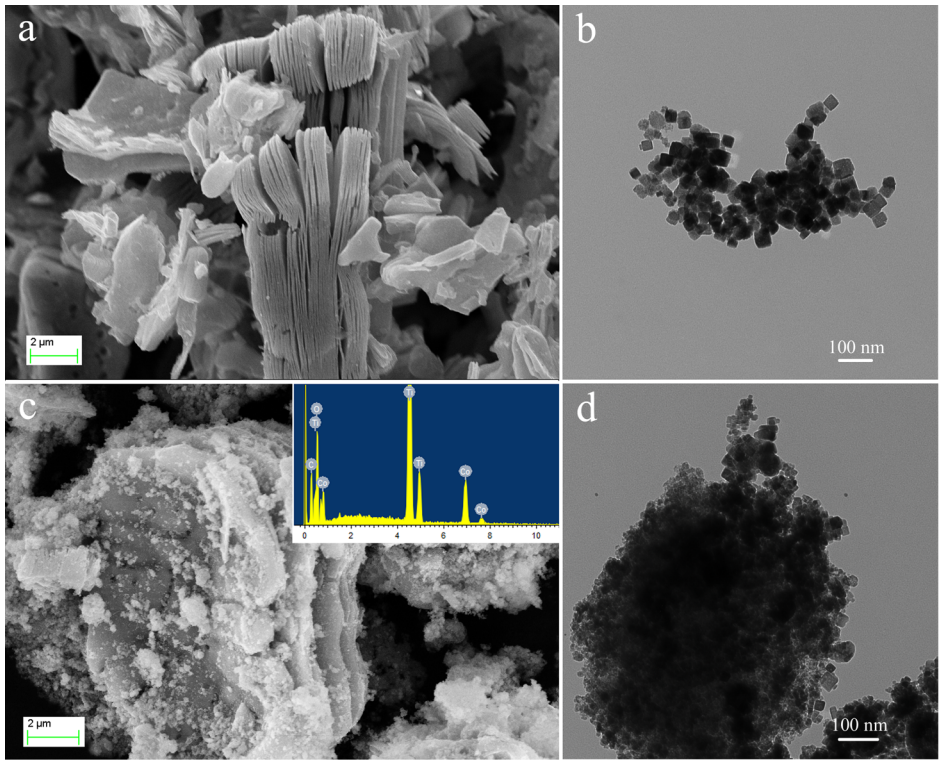

Figure 2. (a) Representative SEM image of the layered MXene sample; (b) TEM image of Co_3O_4 sample; (c,d) SEM and TEM images of prepared MXene-Co_3O_4.

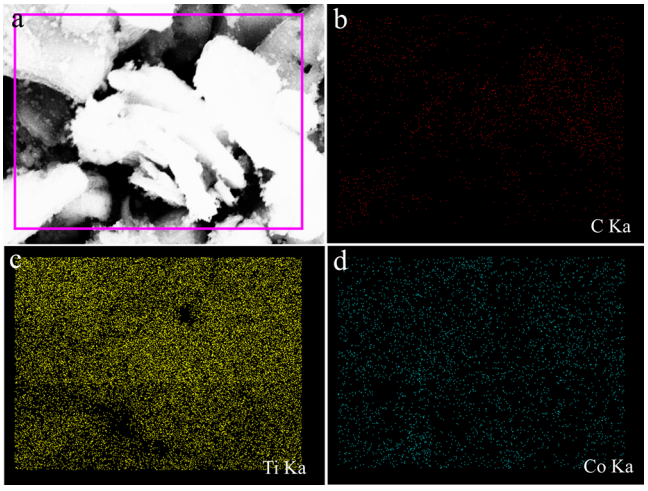

Figure 3. (a) Representative SEM image of the prepared MXene-Co_3O_4 and elemental mapping images of (b) C, (c) Ti, and (d) Co.

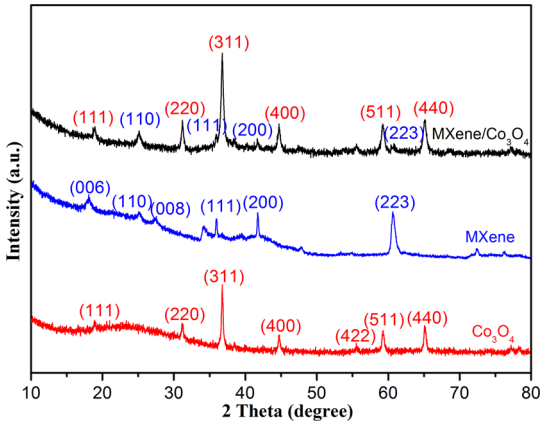

Figure 4. XRD curves of as-prepared MXene, MXene-Co_3O_4, and Co_3O_4.

removal rate, A_0 is defined as the initial absorbance of the supernatant of the dye solution, and A_T is defined as the absorbance of the supernatant of the dye solution collected at different intervals.

In order to compare the performance of the synthesized catalyst, we evaluated the effects of catalytic degradation of dyes (MB and RhB) using two catalysts, respectively. The adsorption kinetic experiments of the as-prepared nanocomposites were carried out using the results of RhB and MB, as shown in Figures 7 and 8. It could be seen that, for MXene-Co_3O_4, the removal rates of MB and RhB were stabilized in about 240 and 80 min, respectively, indicating that the prepared complex acted as an effective dye adsorbent. For Co_3O_4, the MB and RhB removal rates reached stable values in about 200 and 1200 min, respectively. When H_2O_2 was not added, it was clear that the catalyst could hardly degrade the dyes.

In addition, the adsorption kinetic process could be described by classical kinetic models as follows: The pseudo-first-order model could be represented by eq 1

$$\log(q_e - q_t) = \log q_e - \frac{k_1}{2.303}t \quad (1)$$

The pseudo-second-order model could be represented by eq 2

$$\frac{t}{q_t} = \frac{1}{k_2 q_e^{\,2}} + \frac{t}{q_e} \quad (2)$$

DOI: 10.1021/acsomega.9b00231
ACS Omega 2019, 4, 3946−3953

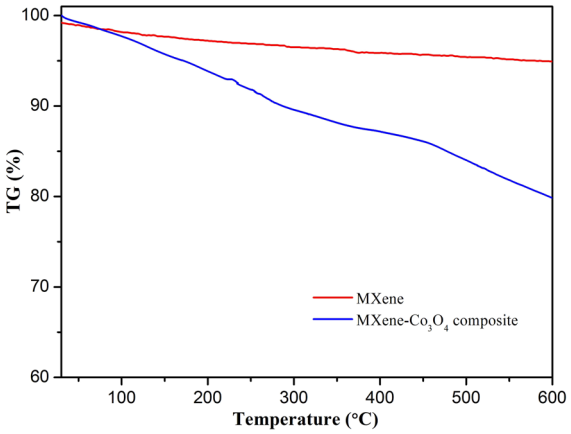

Figure 5. TG curves of MXene and MXene-Co_3O_4 nanocomposites.

where q_e is the equilibrium adsorption capacity (mg/g), q_t is the adsorption capacity at time t (mg/g), and k_1 and k_2 values are the kinetic rate constants.[44−47]

At the same time, Table 1 clearly shows the kinetic results of the experimental data, and the respective fitting parameters were obtained. As shown in Figure 7, by comparing the linear fitting parameters, the pseudo-first-order and pseudo-second-order kinetics of MB and RhB were catalyzed by MXene-Co_3O_4 and Co_3O_4. Based on the above data, it could be easily observed that the obtained MXene-Co_3O_4 composite showed the best adsorption capacity, which could be related to the synergy effect between MXene and Co_3O_4.

2.3. Reasonable Activation Mechanisms of H_2O_2. The discovery of antibiotics derived from natural products has aroused global attention. A promising and challenging method of antibiotic degradation is the Fenton method. This reaction can be carried out at neutral pH, which was an important advantage. A study on oxidative degradation of organic dyes with H_2O_2 had been reported previously.[16] However, the exact mechanism for dye decomposition with H_2O_2 remains unclear. According to a previous study, cobalt-based Fenton/Fenton-like processes could be performed at neutral pH.[18] On the one hand, it was found that homogeneous Co^{2+}/H_2O_2 systems were able to degrade dye contaminants without controlling pH completely.[19] On the other hand, the catalytic decomposition of organic contaminants by heterogeneous Co catalysts under the condition of adding H_2O_2 was also investigated. In a recent study, Co^{2+} adsorbed alumina was used as a heterogeneous catalyst to degrade methylene blue and methyl orange.[17] In those cases, the Co-based heterogeneous catalyst could effectively degrade contaminants at neutral or even alkaline pH. Co-based heterogeneous catalysts could effectively degrade the pollutants at neutral or even basic pH.

$$\equiv Co(II) + H_2O_2 \rightarrow \equiv Co(III) + HO^{\bullet} \quad (3)$$

$$H_2O_2 + HO^{-} \leftrightarrow HO_{2^-} + H_2O \quad (4)$$

$$\equiv Co(III) + HO_{2^-} \rightarrow \equiv Co(II) + HO_2^{\bullet} \quad (5)$$

In contrast, $HO^{\bullet}$ produced by Co^{2+} mediated H_2O_2 activation has been recorded in only a few studies.[18,21] The $HO^{\bullet}$ formation mechanism by Co could be proposed as reactions 3−5. As shown in reaction 3, $HO^{\bullet}$ played an important role in the Co(II)/Co(III) cycle. The ability of MXene-Co_3O_4 in the catalytic process of MB could be attributed to the positive synergistic effect of MXene, MB, and Co_3O_4 with the aid of H_2O_2. First, the cationic MB molecules were easily adsorbed to the surface of MXene due to electrostatic attraction, and the functional groups such as −F and −OH that were rich on the surface of MXene also endowed the excellent catalytic ability during the chemical reaction process.

This adsorption significantly improved the effective concentration of MB molecules anchored on the surface of MXene-Co_3O_4, leading to a high catalytic degradation rate. Second, the hydrophilicity of MXene made the MXene-Co_3O_4 complex well dispersed in water. Good contact between Co_3O_4 nanocomposites and MXene prevented Co_3O_4 from falling off during the catalytic process. The H_2O_2 was then effectively catalyzed to produce free $^{\bullet}OH$ radical species and ultimately promote degradation of the MB molecules. Hence, in terms of MXene-Co_3O_4 composites, there was a coupling between adsorption and catalytic reactions in a single process.[23] Compared to bare MXene and Co_3O_4, the degradations of MB and RhB were significantly increased.

Compared to other nanoparticle catalysts reported, the present prepared composite catalyst could be recovered readily from the solution.[48] After reaching the adsorption equilibrium in the reaction solution, the recovered MXene-Co_3O_4 composite was treated by a thorough cleaning procedure to eliminate possible dye residues and regenerate the catalyst. Through repeated adsorption by using the same catalyst and fresh dye solutions, it could be used in eight consecutive cycles

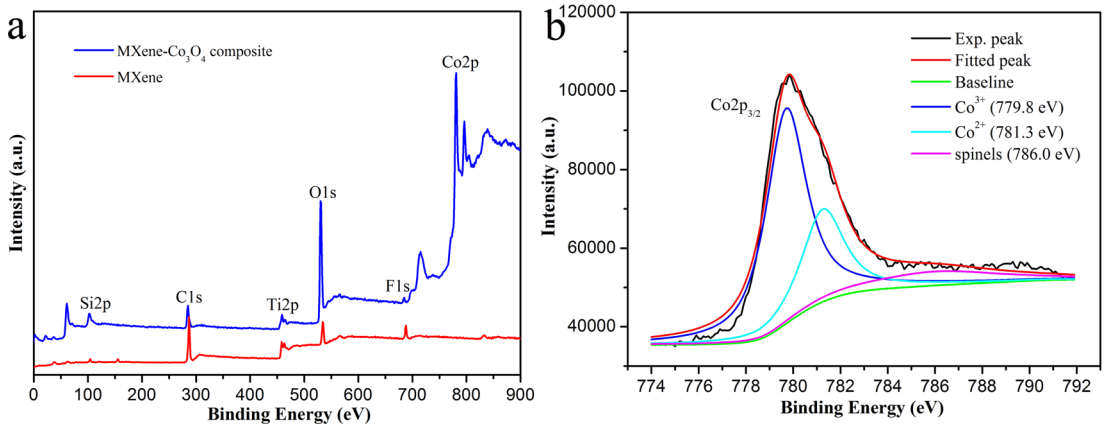

Figure 6. (a) XPS survey spectra of MXene and MXene-Co_3O_4 nanocomposites; (b) high-resolution scan of $Co2p_{3/2}$.

DOI: 10.1021/acsomega.9b00231
ACS Omega 2019, 4, 3946−3953

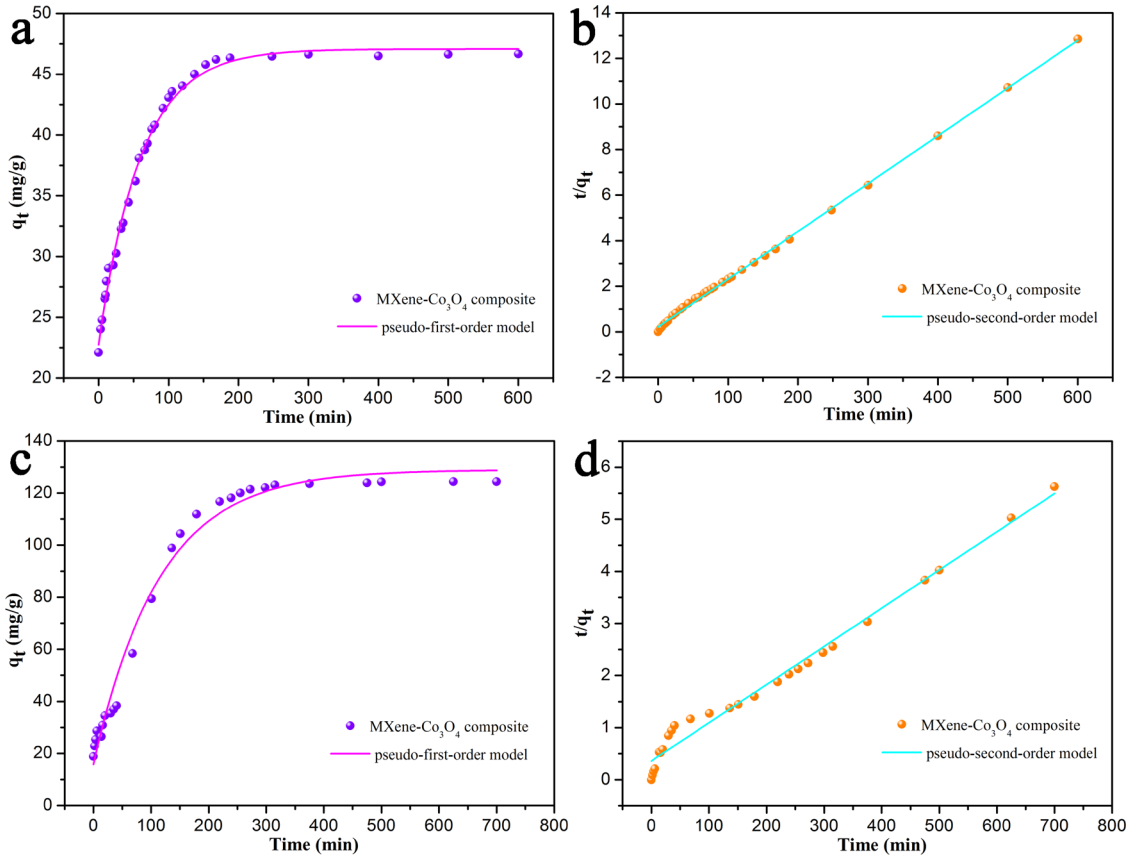

Figure 7. Adsorption kinetic curves of as-prepared MXene-Co_3O_4 nanocomposite on RhB (a,b) and MB (c,d) at 298 K.

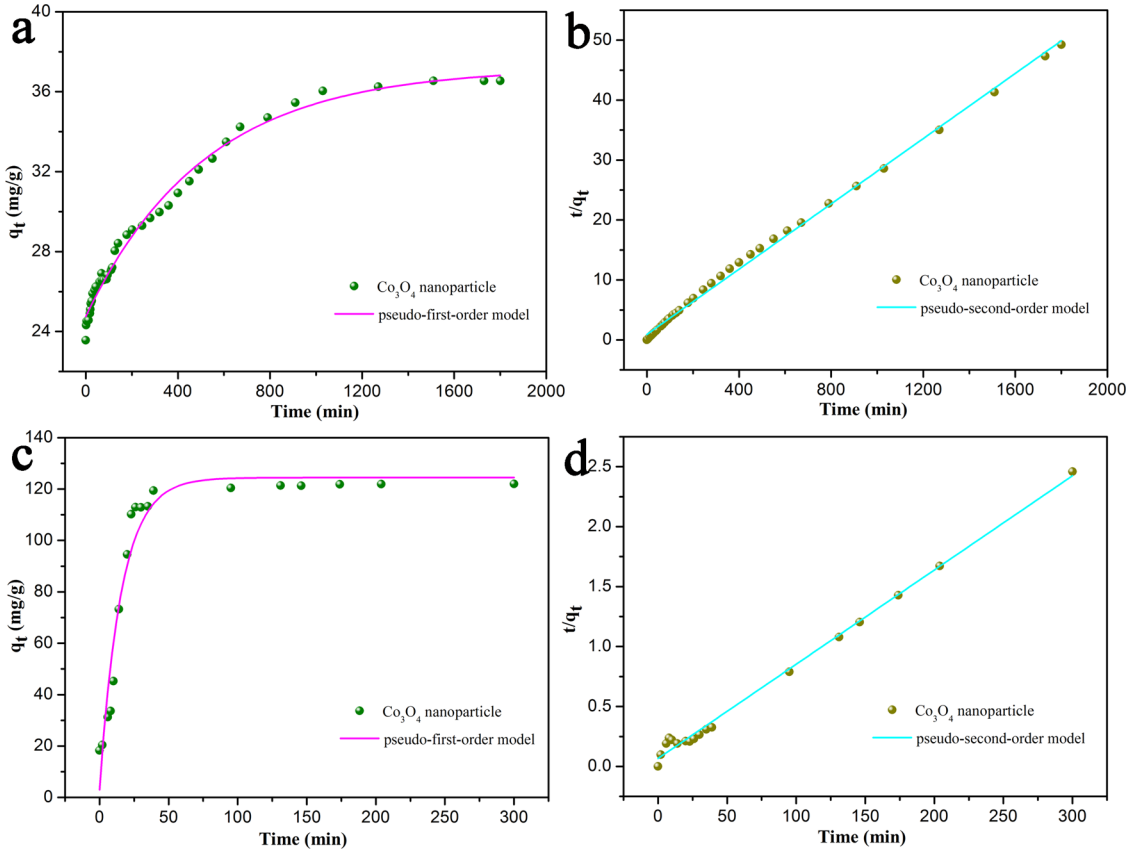

Figure 8. Adsorption kinetic curves of as-prepared Co_3O_4 particles on RhB (a,b) and MB (c,d) at 298 K.

DOI: 10.1021/acsomega.9b00231
ACS Omega 2019, 4, 3946−3953

Table 1. Kinetic Parameters of the Obtained MXene-Co_3O_4 and Co_3O_4 for RhB and MB Removal at 298 K[a]

	pseudo-first-order model			pseudo-second-order model		
catalyst	q_e (mg/g)	R^2	k_1 (min^{-1})	q_e (mg/g)	R^2	k_2 [g/(mg·min)]
RhB						
Mxene-Co_3O_4	47.076	0.99484	1.674×10^{-2}	47.687	0.99910	1.905×10^{-4}
Co_3O_4	37.191	0.98874	1.940×10^{-3}	37.037	0.99748	9.932×10^{-5}
MB						
Mxene-Co_3O_4	128.91	0.98534	8.750×10^{-3}	136.24	0.98391	6.328×10^{-2}
Co_3O_4	124.46	0.94443	6.354×10^{-2}	127.23	0.99479	1.894×10^{-3}

[a]Experimental data from Figures 7 and 8.

(Figure 9). The results showed that, after eight consecutive cycles, the MB removal rate was maintained at about 92.37%.

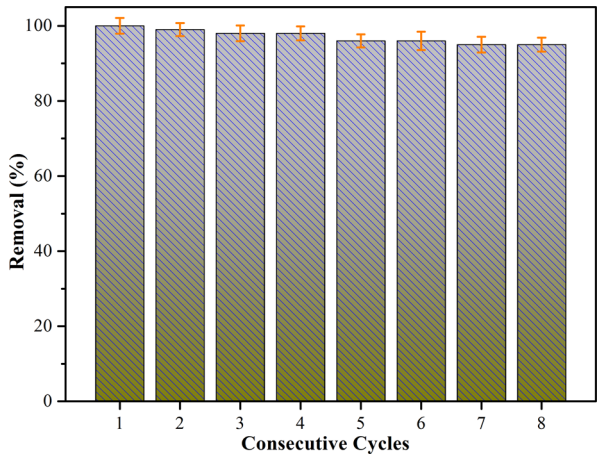

Figure 9. Relative regeneration studies of as-prepared MXene-Co_3O_4 toward MB at room temperature for different consecutive cycles.

The obtained nanocomposites performed well in terms of stability and recyclability. In addition, the reduction of MB degradation could be attributed to the loss and aggregation of the catalyst in the recycling process, as well as the adsorption of MB or intermediates. The above data indicated that the synthesized catalyst could potentially be utilized in pollutant treatment.

3. CONCLUSIONS

In conclusion, we have successfully synthesized a Co_3O_4 nanocrystal-loaded MXene composite by simple in situ solvothermal synthesis. Due to its simple and mild reaction conditions, this simple in situ synthesis method could also be applied to the synthesis of other MXene-based transition metal oxides. The present obtained MXene-Co_3O_4 nanostructure has a very high MB and RhB degradation capacity and well repeatability. After eight consecutive catalytic cycles, the catalytic properties of the sample were still good, showing that the stability and repeatability of Mxene-Co_3O_4 nanocomposites were satisfying. The possible mechanism for adsorbing methylene blue and Rhodamine B to Mxene-Co_3O_4 and Co_3O_4 has been proposed, respectively. The research work showed that the obtained nanocomposites have good and wide applications as new catalytic composite materials.

4. EXPERIMENTAL SECTION

4.1. Materials. Ti_3C_2 (MXene) is obtained by etching a mixed solution of HCl (6 M) and LiF (2.5 M) using Ti_3AlC_2 as a raw material. $Co(CH_3COO)_2{\cdot}4H_2O$ was provided by Aladdin Industrial Corporation, China. Hydrogen peroxide (H_2O_2, 30% in water) was obtained from Kermel Tianjin Chemical Reagent Co., Ltd. Methylene blue (MB) and Rhodamine B (RhB) were obtained from Hubei Mali Ltd., China, and Tianjin Kaitong Chemical Reagent Co., Ltd., respectively. Ethanol (C_2H_5OH) was obtained from Tianjin Kaitong Chemical Reagent Co., Ltd. Deionized (DI) water was used in all experiments.

4.2. Synthesis of the MXene-Co_3O_4 Nanocomposites. Original MXene (20 mg) was dissolved in 4 mL of ultrapure water, and the mixture was sonicated for 0.5 h. Then, 2 mL of 0.2 M $Co(Ac)_2$ solution was added dropwise, 20 mL of ethanol was added, and the solution was magnetically stirred for 2 h. Then, the above reaction solution was poured into a 100 mL Teflon-lined steel autoclave. The autoclave was then heated at 120 °C for 8 h. After cooling down to room temperature and centrifugation, the final obtained precipitate was washed three times with ethanol and lyophilized to obtain the desired MXene-Co_3O_4 composites.

4.3. Preparation of Co_3O_4 Nanoparticles. The synthesis of pure Co_3O_4 samples was similar to the preparation of MXene-Co_3O_4 by reducing the addition of MXene of the same quality. Ethanol (20 mL) was added to 2 mL of 0.2 M $Co(Ac)_2$ solution and stirred for 2 h. Then, the mixture was transferred to a 100 mL steel autoclave reactor and heated at 120 °C for 8 h.

4.4. Characterization. Thermogravimetric analysis (TGA) was tested in an argon environment by a NETZSCH STA 409 PC Luxx simultaneous thermal analyzer (Netzsch Instruments Manufacturing Co., Ltd., Germany). X-ray photoelectron spectroscopy (XPS) was measured by the Thermo Scientific ESCALab 250Xi with an Al Kα X-ray source. The adsorption experiments were monitored by using a Shimadzu UV2550 spectrophotometer. All aqueous solutions were prepared with water purified in a double-stage Millipore Milli-Q Plus purification system. The morphologies were obtained by using a transmission electron microscope (TEM) (HT7700, Hitachi High-Technologies Corporation, Japan) with an accelerating voltage of 20 kV. X-ray diffraction (XRD) analysis was recorded with an X-ray diffractometer (SMART LAB, Rigaku, Japan). The microstructures of the samples were characterized by using a field-emission scanning electron microscope (SEM) (S-4800II, Hitachi, Japan) equipped with energy dispersive X-ray spectroscopy (EDS). Absorption spectra were measured with a LabTech UV-2100 ultraviolet−visible (UV−vis) spectrophotometer.

DOI: 10.1021/acsomega.9b00231
ACS Omega 2019, 4, 3946−3953

4.5. Catalytic Test of MXene-Co_3O_4 Nanocomposites.

In order to evaluate the catalytic performance of the obtained materials, we assessed the performance by degradation of methylene blue and Rhodamine B.[49,50] The prepared Mxene-Co_3O_4 composites (10 mg) and 15 mL of H_2O_2 solution (30% in water) were added to the Rhodamine B and methylene blue solution. A small sample amount of the suspension was taken at regular intervals, and the absorbance of the sample was measured by using a UV−vis spectrophotometer. Moreover, cyclic stability of the catalyst was evaluated by eight replicate experiments. At time t (min), the dye adsorption amount q_t (mg/g) per unit mass of catalyst was calculated by the following formula

$$q_t = \frac{(C_0 - C_t)V}{m} \quad (6)$$

where C_0 is the initial concentration of the adsorption solution (mg/L), C_t is the concentration of the adsorption solution at time t (mg/L), m is the total amount of the sample (g), and V is the volume of the adsorption solution (L).

AUTHOR INFORMATION

Corresponding Author

*E-mail: tfjiao@ysu.edu.cn.

ORCID

Tifeng Jiao: 0000-0003-1238-0277

Qiuming Peng: 0000-0002-3053-7066

Notes

The authors declare no competing financial interest.

ACKNOWLEDGMENTS

We greatly appreciate the financial support of the National Natural Science Foundation of China (No. 21872119), the Support Program for the Top Young Talents of Hebei Province, the China Postdoctoral Science Foundation (No. 2015M580214), the Research Program of the College Science & Technology of Hebei Province (No. ZD2018091), and the Scientific and Technological Research and Development Program of Qinhuangdao City (No. 201701B004).

REFERENCES

(1) Naguib, M.; Kurtoglu, M.; Presser, V.; Lu, J.; Niu, J.; Heon, M.; Hultman, L.; Gogotsi, Y.; Barsoum, M. W. Two-dimensional nanocrystals produced by exfoliation of Ti_3AlC_2. *Adv. Mater.* **2011**, *23*, 4248−4253.

(2) Li, Z.; Wang, L.; Sun, D.; Zhang, Y.; Liu, B.; Hu, Q.; Zhou, A. Synthesis and thermal stability of two-dimensional carbide MXene Ti_3C_2. *Mater. Sci. Eng. B* **2015**, *191*, 33−40.

(3) Khazaei, M.; Ranjbar, A.; Arai, M.; Sasaki, T.; Yunoki, S. Electronic properties and applications of MXenes: a theoretical review. *J. Mater. Chem. C* **2017**, *5*, 2488−2503.

(4) Li, K.; Jiao, T.; Xing, R.; Zou, G.; Zhou, J.; Zhang, L.; Peng, Q. Fabrication of tunable hierarchical MXene@AuNPs nanocomposites constructed by self-reduction reactions with enhanced catalytic performances. *Sci. China Mater.* **2018**, *61*, 728−736.

(5) Naguib, M.; Kurtoglu, M.; Presser, V.; Lu, J.; Niu, J.; Heon, M.; Hultman, L.; Gogotsi, Y.; Barsoum, M. W. Two-dimensional nanocrystals: two-dimensional nanocrystals produced by exfoliation of Ti_3AlC_2. *Adv. Mater.* **2011**, *23*, 4207−4207.

(6) Srivastava, P.; Mishra, A.; Mizuseki, H.; Lee, K.-R.; Singh, A. K. Mechanistic insight into the chemical exfoliation and functionalization of Ti_3C_2 MXene. *ACS Appl. Mater. Interfaces* **2016**, *8*, 24256−24264.

(7) Mishra, A.; Srivastava, P.; Mizuseki, H.; Lee, K.-R.; Singh, A. K. Isolation of pristine MXene from Nb_4AlC_3 MAX phase: a first-principles study. *Phys. Chem. Chem. Phys.* **2016**, *18*, 11073−11080.

(8) Naguib, M.; Mochalin, V. N.; Barsoum, M. W.; Gogotsi, Y. 25th anniversary article: MXenes: A new family of two-dimensional materials. *Adv. Mater.* **2014**, *26*, 992−1005.

(9) Zhang, E.; Xie, Y.; Ci, S.; Jia, J.; Wen, Z. Porous Co_3O_4 hollow nanododecahedra for nonenzymatic glucose biosensor and biofuel cell. *Biosens. Bioelectron.* **2016**, *81*, 46−53.

(10) Cheng, G.; Kou, T.; Zhang, J.; Si, C.; Gao, H.; Zhang, Z. O_2^{2-}/O^- functionalized oxygen-deficient Co_3O_4 nanorods as high performance supercapacitor electrodes and electrocatalysts towards water splitting. *Nano Energy* **2017**, *38*, 155−166.

(11) Huang, X.; Wang, R.; Jiao, T.; Zou, G.; Zhan, F.; Yin, J.; Zhang, L.; Zhou, J.; Peng, Q. Facile Preparation of Hierarchical AgNP-Loaded MXene/Fe_3O_4/Polymer Nanocomposites by Electrospinning with Enhanced Catalytic Performance for Wastewater Treatment. *ACS Omega* **2019**, *4*, 1897−1906.

(12) Yang, X.; Chen, J.; Chen, Y.; Feng, P.; Lai, H.; Li, J.; Luo, X. Novel Co_3O_4 nanoparticles/nitrogen-doped carbon composites with extraordinary catalytic activity for oxygen evolution reaction (OER). *Nano-Micro Lett.* **2018**, *10*, 15.

(13) Chen, Y. M.; Yu, L.; Lou, X. W. Hierarchical tubular structures composed of Co_3O_4 hollow nanoparticles and carbon nanotubes for lithium storage. *Angew. Chem., Int. Ed.* **2016**, *55*, 5990−5993.

(14) Zhang, P.; Zhan, Y.; Cai, B.; Hao, C.; Wang, J.; Liu, C.; Meng, Z.; Yin, Z.; Chen, Q. Shape-controlled synthesis of Mn_3O_4 nanocrystals and their catalysis of the degradation of methylene blue. *Nano Res.* **2010**, *3*, 235−243.

(15) Cheng, M.; Zeng, G.; Huang, D.; Lai, C.; Liu, Y.; Zhang, C.; Wan, J.; Hu, L.; Zhou, C.; Xiong, W. Efficient degradation of sulfamethazine in simulated and real wastewater at slightly basic pH values using Co-SAM-SCS /H_2O_2 Fenton-like system. *Water Res.* **2018**, *138*, 7−18.

(16) Liu, Y.; Wang, J. Degradation of sulfamethazine by gamma irradiation in the presence of hydrogen peroxide. *J. Hazard. Mater.* **2013**, *250−251*, 99−105.

(17) Mahamallik, P.; Pal, A. Photo-Fenton process in a Co(II)-adsorbed micellar soft-template on an alumina support for rapid methylene blue degradation. *RSC Adv.* **2016**, *6*, 100876−100890.

(18) Bokare, A. D.; Choi, W. Review of iron-free Fenton-like systems for activating H_2O_2 in advanced oxidation processes. *J. Hazard. Mater.* **2014**, *275*, 121−135.

(19) Ling, S. K.; Wang, S.; Peng, Y. Oxidative degradation of dyes in water using Co^{2+}/H_2O_2 and Co^{2+}/peroxymonosulfate. *J. Hazard. Mater.* **2010**, *178*, 385−389.

(20) Ding, D.; Wang, Y.; Li, X.; Qiang, R.; Xu, P.; Chu, W.; Han, X.; Du, Y. Rational design of core-shell Co@C microspheres for high-performance microwave absorption. *Carbon* **2017**, *111*, 722−732.

(21) Yan, Z.; Hu, Q.; Yan, G.; Li, H.; Shih, K.; Yang, Z.; Li, X.; Wang, Z.; Wang, J. Co_3O_4/Co nanoparticles enclosed graphitic carbon as anode material for high performance Li-ion batteries. *Chem. Eng. J.* **2017**, *321*, 495−501.

(22) Huo, S.; Duan, P.; Jiao, T.; Peng, Q.; Liu, M. Self-assembled luminescent quantum dots to generate full-color and white circularly polarized light. *Angew. Chem., Int. Ed.* **2017**, *56*, 12174−12178.

(23) Yanalak, G.; Aljabour, A.; Aslan, E.; Ozel, F.; Patir, I. H.; Kus, M.; Ersoz, M. NiO and Co_3O_4 nanofiber catalysts for the hydrogen evolution reaction at liquid/liquid interfaces. *Electrochim. Acta* **2018**, *291*, 311−318.

(24) Lin, Z.; Qiao, X. Coral-like Co_3O_4 decorated N-doped carbon particles as active materials for oxygen reduction reaction and supercapacitor. *Sci. Rep.* **2018**, *8*, 1802.

(25) Yin, Y.; Ma, N.; Xue, J.; Wang, G.; Liu, S.; Li, H.; Guo, P. Insights into the role of poly(vinylpyrrolidone) in the synthesis of palladium nanoparticles and their electrocatalytic properties. *Langmuir* **2019**, *35*, 787−795.

(26) Xing, R.; Liu, K.; Jiao, T.; Zhang, N.; Ma, K.; Zhang, R.; Zou, Q.; Ma, G.; Yan, X. An Injectable Self-Assembling Collagen-Gold

DOI: 10.1021/acsomega.9b00231
ACS Omega 2019, 4, 3946−3953

Hybrid Hydrogel for Combinatorial Antitumor Photothermal/Photodynamic Therapy. *Adv. Mater.* **2016**, *28*, 3669−3676.
(27) Chen, K.; Jiao, T.; Li, J.; Han, D.; Wang, R.; Tian, G.; Peng, Q. Chiral Nanostructured Composite Films via Solvent-Tuned Self-Assembly and Their Enantioselective Performances. *Langmuir*, in press, DOI: 10.1021/acs.langmuir.9b00014.
(28) Wang, C.; Yin, J.; Wang, R.; Jiao, T.; Huang, H.; Zhou, J.; Zhang, L.; Peng, Q. Facile preparation of self-assembled polydopamine-modified electrospun fibers for highly effective removal of organic dyes. *Nanomaterials* **2019**, *9*, 116.
(29) Guo, R.; Wang, R.; Yin, J.; Jiao, T.; Huang, H.; Zhao, X.; Zhang, L.; Li, Q.; Zhou, J.; Peng, Q. Fabrication and highly efficient dye removal characterization of beta-cyclodextrin-based composite polymer fibers by electrospinning. *Nanomaterials* **2019**, *9*, 127.
(30) Xing, R.; Wang, W.; Jiao, T.; Ma, K.; Zhang, Q.; Hong, W.; Qiu, H.; Zhou, J.; Zhang, L.; Peng, Q. Bioinspired polydopamine sheathed nanofibers containing carboxylate graphene oxide nanosheet for high-efficient dyes scavenger. *ACS Sustainable Chem. Eng.* **2017**, *5*, 4948−4956.
(31) Liu, Y.; Hou, C.; Jiao, T.; Song, J.; Zhang, X.; Xing, R.; Zhou, J.; Zhang, L.; Peng, Q. Self-assembled AgNP-containing nanocomposites constructed by electrospinning as efficient dye photocatalyst materials for wastewater treatment. *Nanomaterials* **2018**, *8*, 35.
(32) Wang, C.; Sun, S.; Zhang, L.; Yin, J.; Jiao, T.; Zhang, L.; Xu, Y.; Zhou, J.; Peng, Q. Facile preparation and catalytic performance characterization of AuNPs-loaded hierarchical electrospun composite fibers by solvent vapor annealing treatment. *Colloids Surf., A* **2019**, *561*, 283−291.
(33) Sun, S.; Wang, C.; Han, S.; Jiao, T.; Wang, R.; Yin, J.; Li, Q.; Wang, Y.; Geng, L.; Yu, X.; Peng, Q. Interfacial nanostructures and acidichromism behaviors in self-assembled terpyridine derivatives Langmuir-Blodgett films. *Colloids Surf., A* **2019**, *564*, 1−9.
(34) Huang, X.; Jiao, T.; Liu, Q.; Zhang, L.; Zhou, J.; Li, B.; Peng, Q. Hierarchical electrospun nanofibers treated by solvent vapor annealing as air filtration mat for high-efficiency PM2.5 capture. *Sci. China Mater.* **2019**, *62*, 423−436.
(35) Xu, Y.; Ren, B.; Wang, R.; Zhang, L.; Jiao, T.; Liu, Z. Facile preparation of rod-like MnO nanomixtures via hydrothermal approach and highly efficient removal of methylene blue for wastewater Treatment. *Nanomaterials* **2019**, *9*, 10.
(36) Zhan, F.; Wang, R.; Yin, J.; Han, Z.; Zhang, L.; Jiao, T.; Zhou, J.; Zhang, L.; Peng, Q. Facile solvothermal preparation of Fe_3O_4−Ag nanocomposite with excellent catalytic performance. *RSC Adv.* **2019**, *9*, 878−883.
(37) Zhou, J.; Gao, F.; Jiao, T.; Xing, R.; Zhang, L.; Zhang, Q.; Peng, Q. Selective Cu(II) ion removal from wastewater via surface charged self-assembled polystyrene-Schiff base nanocomposites. *Colloids Surf., A* **2018**, *545*, 60−67.
(38) Luo, X.; Ma, K.; Jiao, T.; Xing, R.; Zhang, L.; Zhou, J.; Li, B. Graphene oxide-polymer composite Langmuir films constructed by interfacial thiol-ene photopolymerization. *Nanoscale Res. Lett.* **2017**, *12*, 99.
(39) Chen, K.; Li, J.; Zhang, L.; Xing, R.; Jiao, T.; Gao, F.; Peng, Q. Facile synthesis of self-assembled carbon nanotubes/dye composite films for sensitive electrochemical determination of Cd(II) ions. *Nanotechnology* **2018**, *29*, 445603.
(40) Chandra, V.; Park, J.; Chun, Y.; Lee, J. W.; Hwang, I.-C.; Kim, K. S. Water-dispersible magnetite-reduced graphene oxide composites for arsenic removal. *ACS Nano* **2010**, *4*, 3979−3986.
(41) Wang, H.; Xiang, X.; Li, F. Facile synthesis and novel electrocatalytic performance of nanostructured Ni−Al layered double hydroxide/carbon nanotube composites. *J. Mater. Chem.* **2010**, *20*, 3944−3952.
(42) Li, Y.; Zhao, Y.; Cheng, H.; Hu, Y.; Shi, G.; Dai, L.; Qu, L. Nitrogen-doped graphene quantum dots with oxygen-rich functional groups. *J. Am. Chem. Soc.* **2012**, *134*, 15−18.
(43) Guo, R.; Jiao, T.; Li, R.; Chen, Y.; Guo, W.; Zhang, L.; Zhou, J.; Zhang, Q.; Peng, Q. Sandwiched Fe_3O_4/carboxylate graphene oxide nanostructures constructed by layer-by-layer assembly for highly efficient and magnetically recyclable dye removal. *ACS Sustainable Chem. Eng.* **2018**, *6*, 1279−1288.
(44) Liu, K.; Yuan, C.; Zou, Q.; Xie, Z.; Yan, X. Self-Assembled Zinc/Cystine-Based Chloroplast Mimics Capable of Photoenzymatic Reactions for Sustainable Fuel Synthesis. *Angew. Chem. Int. Ed.* **2017**, *56*, 7876−7880.
(45) Liu, K.; Xing, R.; Li, Y.; Zou, Q.; Möhwald, H.; Yan, X. Mimicking primitive photobacteria: sustainable hydrogen evolution based on peptide-porphyrin co-assemblies with a self-mineralized reaction center. *Angew. Chem., Int. Ed.* **2016**, *55*, 12503−12507.
(46) Liu, K.; Xing, R.; Chen, C.; Shen, G.; Yan, L.; Zou, Q.; Ma, G.; Möhwald, H.; Yan, X. Peptide-induced hierarchical long-range order and photocatalytic activity of porphyrin assemblies. *Angew. Chem., Int. Ed.* **2015**, *54*, 500−505.
(47) Zou, Q.; Liu, K.; Abbas, M.; Yan, X. Peptide-Modulated Self-Assembly of Chromophores toward Biomimetic Light-Harvesting Nanoarchitectonics. *Adv. Mater.* **2016**, *28*, 1031−1043.
(48) Wang, Y.; Zhu, L.; Yang, X.; Shao, E.; Deng, X.; Liu, N.; Wu, M. Facile synthesis of three-dimensional Mn_3O_4 hierarchical microstructures and their application in the degradation of methylene blue. *J. Mater. Chem. A* **2015**, *3*, 2934−2941.
(49) Li, R.; Zhou, D.; Luo, J.; Xu, W.; Li, J.; Li, S.; Cheng, P.; Yuan, D. The urchin-like sphere arrays Co_3O_4 as a bifunctional catalyst for hydrogen evolution reaction and oxygen evolution reaction. *J. Power Sources* **2017**, *341*, 250−256.
(50) Zhai, T.; Wan, L.; Sun, S.; Chen, Q.; Sun, J.; Xia, Q.; Xia, H. Phosphate ion functionalized Co_3O_4 ultrathin nanosheets with greatly improved surface reactivity for high performance pseudocapacitors. *Adv. Mater.* **2017**, *29*, 1604167.

DOI: 10.1021/acsomega.9b00231
ACS Omega 2019, 4, 3946−3953